Research Article

Chang-Qiao Yang* and Su-Qin Li*

Kinetics of iron removal from quartz under ultrasound-assisted leaching

https://doi.org/10.1515/htmp-2020-0081
received December 12, 2019; accepted July 18, 2020

Abstract: Kinetics of iron removal from quartz under the ultrasound-assisted leaching was explored in this paper, and the effects of temperature, leaching time, stirring speed and ultrasonic input power on iron removal were studied. The results revealed that the reaction kinetics followed the shrinking core model and the product layer internal diffusion was the rate-determining step in the ultrasound-assisted leaching process. The activation energy of the ultrasonic-assisted leaching reaction was 27.72 kJ/mol, which was 7.28 kJ/mol higher than that of the regular method. Moreover, the kinetic equation and mathematical model of iron removal from quartz were established. Compared with the regular leaching, only 40 min were required for the ultrasound-assisted leaching process to achieve an iron removal rate of up to 74%. Under the optimal parameters, SiO_2 content of concentrate increased from 99.5828% to 99.9047%, and Fe_2O_3 content reduced from 0.0857% to 0.0223%. Additionally, it was found that the iron removal rate increased with increasing temperature, stirring speed or ultrasonic power.

Keywords: highly pure silica, oxalic acid, shrinking core model, activation energy, mathematical model

1 Introduction

Highly pure quartz is an important nonmetallic high-tech raw material. It is extensively used in manufacturing solar cells, microelectronics components, optical fibers, refractories and high-quality ceramics as well as in other industries [1–3]. Iron oxides in quartz are detrimental impurities, and they can lead to an unacceptable coloring of the final products [4]. In general, it is very difficult to remove the iron impurities embedded in quartz particles, attached to quartz surface or wrapped in gas–liquid inclusions [5]. Various physical, physicochemical or chemical methods have been developed to realize the efficient removal of iron from quartz [6–8]. Among these, chemical processing is considered as the most effective iron removal technique. However, chemical methods are usually expensive and have adverse effects on the environmental safety. In view of these limitations, more environmentally benign reagents or methods should be developed to promote the extensive application of these chemical methods.

In recent years, weak organic acids (such as oxalic acid $H_2C_2O_4$, citric acid $C_6H_8O_7$ and ascorbic acid $C_6H_8O_6$) have been widely used as the substitutes of inorganic acids in the treatment of iron impurities. Tuncuk and Akcil [9] summarized the acid leaching efficiency of various reagents (including inorganic and organic acids) and considered $H_2C_2O_4$ as the most promising leaching reagent because of its good complexing characteristic and high reducing power. Meanwhile, $H_2C_2O_4$ is less harmful to the environment compared to hydrofluoric acid and can be obtained cheaply as a by-product from other industrial processes. In addition to the improvement in terms of leaching reagents, some advances have also been made in the process design. For example, Du et al. [10] investigated the effects of ultrasound on leaching efficiency and found that ultrasonic-assisted acid leaching could significantly increase the iron removal rate. The results of their study showed that the maximum iron removal rate under the ultrasound-assisted acid leaching was 75.4%, which increased by 16.3% in comparison with

* **Corresponding author: Chang-Qiao Yang,** National-Provincial Joint Engineering Research Center for Comprehensive Utilization of Symbiotic-Associated Mineral Waste Resources in Bayan Obo, Inner Mongolia University of Science and Technology, Baotou, 014010, China, e-mail: yangchangqiao@21cn.com
* **Corresponding author: Su-Qin Li,** School of Metallurgical and Ecological Engineering, University of Science and Technology Beijing, Beijing, 100083, China, e-mail: ustblisuqin@126.com

that without ultrasound. Moreover, it was found that the iron oxides on the surface of quartz particles could be eliminated more efficiently by ultrasound than by mechanical scrubbing [11]. Overall, ultrasound treatment can improve the iron removal kinetics [12,13], but the kinetics of iron removal in the leaching process has not been presented by these authors.

Cornell and Schindler [14] studied the kinetics of photochemical dissolution of goethite in $H_2C_2O_4$ solution and suggested that both protons and oxalate ions participated in the dissolution reaction. Liu et al. [15] investigated the leaching kinetics of Chinese laterite containing maghemite and magnetite in sulfuric acid (H_2SO_4) solution, and their results showed that temperature, acid concentration and particle size had significant effects on the leaching efficiency. The leaching kinetics followed the shrinking core model; and the rate-determining step changed from surface chemical reaction in the early and middle stages to internal diffusion in the later stage.

Taxiarchou et al. [16] studied the dissolution kinetics of hematite in $H_2C_2O_4$ solution and found that the dissolution process was much faster in an inert atmosphere. Their results showed that iron dissolution was highly dependent on temperature and pH value of the mother liqueur but not affected by $H_2C_2O_4$ concentration. Lee et al. [17,18] investigated the kinetics of iron oxide leaching by $H_2C_2O_4$ and found that the dissolution of hematite and magnetite at pH of 2.5–3.0 followed the shrinking core model controlled by the product layer diffusion. The dissolution reaction was very slow in the temperature range of 25–60°C, but its rate increased rapidly above 90°C. Besides, they also reported that the reaction rate increased with increasing $H_2C_2O_4$ concentration, which was inconsistent with Taxiarchou's results. Olvera-Venegas et al. [19] studied the effects of temperature and acid concentration on the dissolution of ilmenite, greigite, and magnetite. The authors found that the temperature had the most significant effect on the iron dissolution, while $C_6H_8O_7$ concentration moderately affected the dissolution process. The kinetics of iron dissolution could be described by the shrinking core model, and the chemical reaction was determined as the controlling step.

Salmimies et al. [20] studied the kinetics of magnetite dissolution in mixtures of $H_2C_2O_4$ and H_2SO_4 considered the Kabai model as the most appropriate for describing the dissolution kinetics. The reaction rate constant k at 35°C was found to vary between $4.1 \times 10^{-5}\,s^{-1}$ and $5.6 \times 10^{-4}\,s^{-1}$ for different acid concentrations, and the kinetics could be significantly improved by increasing $H_2C_2O_4$ concentration from 50 to 70%.

Some scholars believed [21–24] that the iron extraction kinetics followed the shrinking core model in acid solutions. However, there are still controversies about the effects of temperature, acid concentration and other parameters on the leaching efficiency. In addition, the rate-determining step is also not determined yet. To the best of our knowledge, few published reports are available about the iron dissolution kinetics under the ultrasound-assisted leaching.

In this study, the removal of iron oxides in mixtures of $H_2C_2O_4$ and HCl is investigated to determine the effects of various parameters such as temperature, stirring speed, leaching time and ultrasonic input power on the iron removal efficiency. Additionally, the rate-determining step is discussed based on the shrinking core model under the ultrasound-assisted leaching or without the ultrasound. On this basis, a mathematical model is developed to provide the potential optimum conditions for iron removal.

2 Materials and methods

2.1 Raw materials, instrumentation and reagents

The quartz samples in this investigation were purchased from Lianyungang Xinhai Quartz Products Co., Ltd located in Lianyungang City of Jiangsu Province, China. The complete chemical compositions of the samples were determined by X-ray fluorescence (XRF; Axios mAX, the Netherlands PANalytical) and the results are presented in Table 1.

Table 1: The chemical composition of original samples by XRF (%)[a]

Components	SiO_2	Al_2O_3	Fe_2O_3	CaO	Na_2O	K_2O	MgO
Amount	99.5828	0.1158	0.0857	0.0422	0.0387	0.0355	0.0327

[a] The oxides of less than 0.03% are not shown.

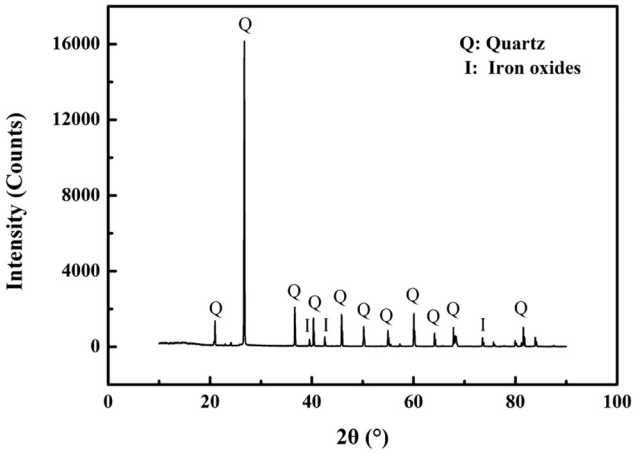

Figure 1: The X-ray diffractogram of quartz samples.

In order to know the mineralogy of the samples, X-ray diffraction (XRD; D/max 2550PC, Japan Rigaku Co., Ltd, with Cu-K_α radiation between 10° and 90°) was used, and the XRD pattern is shown in Figure 1. As can be seen, the samples show a very high percentage of quartz and a very small amount of iron oxides, implying the purity of these quartz samples is very high. The result is in good agreement with the XRF result.

Iron content of the quartz was examined by ICP-OES (Varian 715-ES, USA). The particle size and size distribution of the samples were determined by laser light scattering method (Mastersizer 2000, Malvern, UK).

All the used chemical reagents were analytically pure and were produced by Sinopharm Group Chemical Reagent Co., Ltd., China. Deionized water (laboratory production) was used throughout this study.

2.2 Experimental

2.2.1 Regular acid leaching experiment

The leaching agent was prepared by dissolving known amounts of $H_2C_2O_4$ and HCl in the deionized water. The prepared leaching agent was heated up to a desired temperature and 20 g dry quartz samples were immediately added into the hot liquid under continuous stirring. To prevent evaporation, the glass extraction vessel was closed throughout the leaching experiment. When the reaction was completed, the filtrate was drained and the residue was taken out. The residue was washed in the deionized water to achieve neutral pH. Then it was filtered onto the filter paper and dried for subsequent composition analysis.

2.2.2 Ultrasonic-assisted acid leaching experiment

The ultrasonic-assisted experiment was conducted according to the same procedure as described above. The only difference was that an ultrasound cell breaker probe was immersed into the liquid to be extracted in the glass extraction vessel. Different input powers and treatment times were examined. After the desired extraction time, the same washing procedure was implemented as presented in Section 2.2.1.

All experiments were carried out at least twice and the mean values were taken as the final results. Figure 2 shows the schematic diagram of the experimental setup.

2.3 Evaluation and characterization

The iron removal rate was calculated using the following equation:

$$x = \left(1 - \frac{\theta}{\alpha}\right) \times 100\% \quad (1)$$

where x is the iron removal rate, θ is the amount of iron in the leached solid sample and α is the amount of iron in ore sample.

3 Results and discussion

3.1 Kinetic analysis of iron leaching process

The shrinking core model is the most commonly used liquid–solid phase non-catalytic reaction model [25].

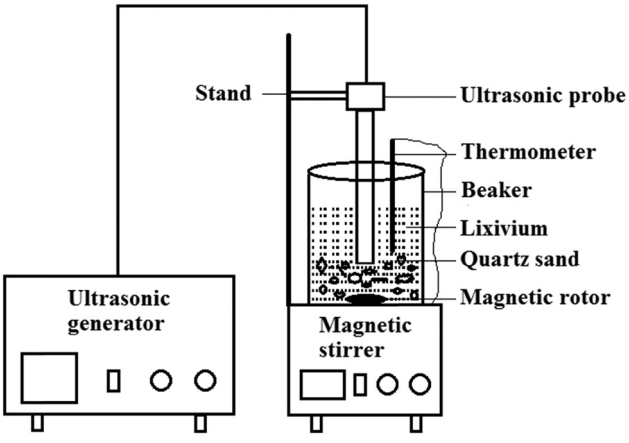

Figure 2: Schematic diagram of the experimental setup.

In the interface reaction model without solid products, the reaction occurs only at the interface of the liquid and solid phases, and the reaction surface shrinks continuously from the surface to the center of the solid particle. The whole reaction process involves the following five steps.

$$aA(l) + bB(s) = cC(l) + dD(s) \quad (2)$$

Step 1: External diffusion process of the reaction. The liquid reactant *A* goes through the fluid body and passes through the fluid film outside the particle surface to the solid particle surface.

Step 2: Internal diffusion process of the reactant. The liquid reactant *A* goes through the solid product layer and then diffuses to the reaction interface.

Step 3: Interface chemical reaction process. The liquid reactant *A* and the solid reactant *B* react at the solid-phase interface.

Step 4: Internal diffusion process of the liquid product. The liquid product *C* diffuses to the outer surface of the particle through the solid product layer.

Step 5: External diffusion process of the liquid product. The liquid product *C* diffuses from the outer surface of the particle to the main fluid body through the stagnant membrane.

The acid leaching reaction of quartz sands belongs to liquid-solid phase reaction. The chemical reaction equations of iron impurities (expressed as Fe_2O_3) with HCl and $H_2C_2O_4$ can be summarized as follows:

$$Fe_2O_3 + 6H^+ \rightarrow 2Fe^{3+} + 3H_2O \quad (3)$$

$$Fe_2O_3 + H^+ + 5HC_2O_4^- \rightarrow 2Fe(C_2O_4)_2^{2-} + 3H_2O + 2CO_2 \quad (4)$$

The above reactions can be considered as liquid-solid phase noncatalytic reactions on the surface of the solid particle. The reaction products Fe^{3+} and $Fe(C_2O_4)_2^{2-}$ can be dissolved in the liquid and SiO_2 is left.

Figure 3 shows the particle size distribution of the samples. The size of the initial quartz sands is between 150 and 350 μm, with an average value of 238.502 μm (Figure 3(a)). After acid leaching, the samples have an average particle size of 234.325 μm (Figure 3(b)), which is very similar to that of the initial samples. It can be found that the particle size is almost unchanged before and after the acid leaching process. Therefore, the shrinking unreacted core model can be used to describe these reaction processes, and in this case, only by the following three steps [26]:

Step 1: External diffusion. Since the reaction system is usually equipped with a stirring device in the acid leaching process, the external diffusion process can be ignored and will not be the rate-determining step.

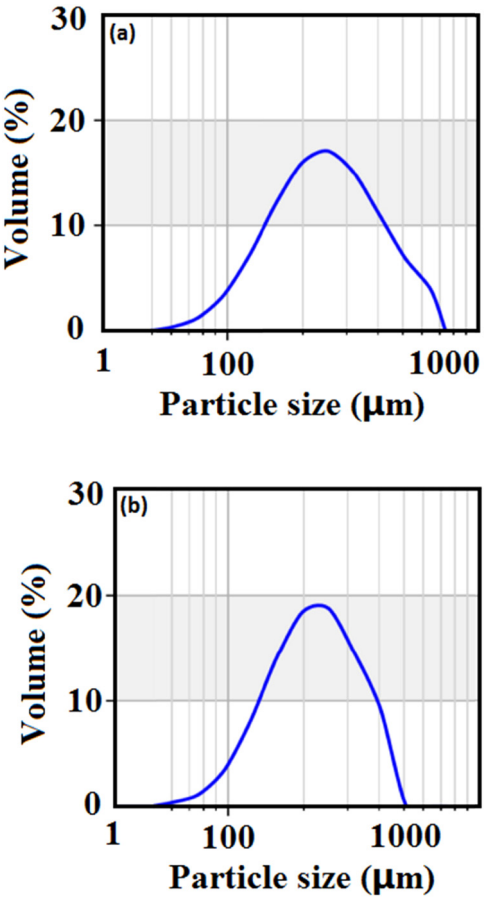

Figure 3: Particle size distribution of (a) original samples, (b) leached solid samples (acid leaching conditions – $H_2C_2O_4$ concentration: 10 g/L, HCl concentration: 5%, temperature: 60°C, L/S ratio: 5, time: 8 h, stirring speed: 500 rpm).

Step 2: Chemical reaction. The kinetic equation can be expressed as:

$$1 - (1 - x)^{1/2} = kt \quad (5)$$

Step 3: Internal diffusion. The kinetic equation can be expressed as:

$$1 - \frac{2}{3}x - (1 - x)^{2/3} = kt \quad (6)$$

where x is the iron removal rate ranging from 0 to 1 (%), k is the reaction rate constant (s^{-1}) and t is time (s).

3.2 Determination of the rate-determining step

Figure 4(a) presents the influence of stirring speed on the iron removal efficiency. It can be seen that the iron

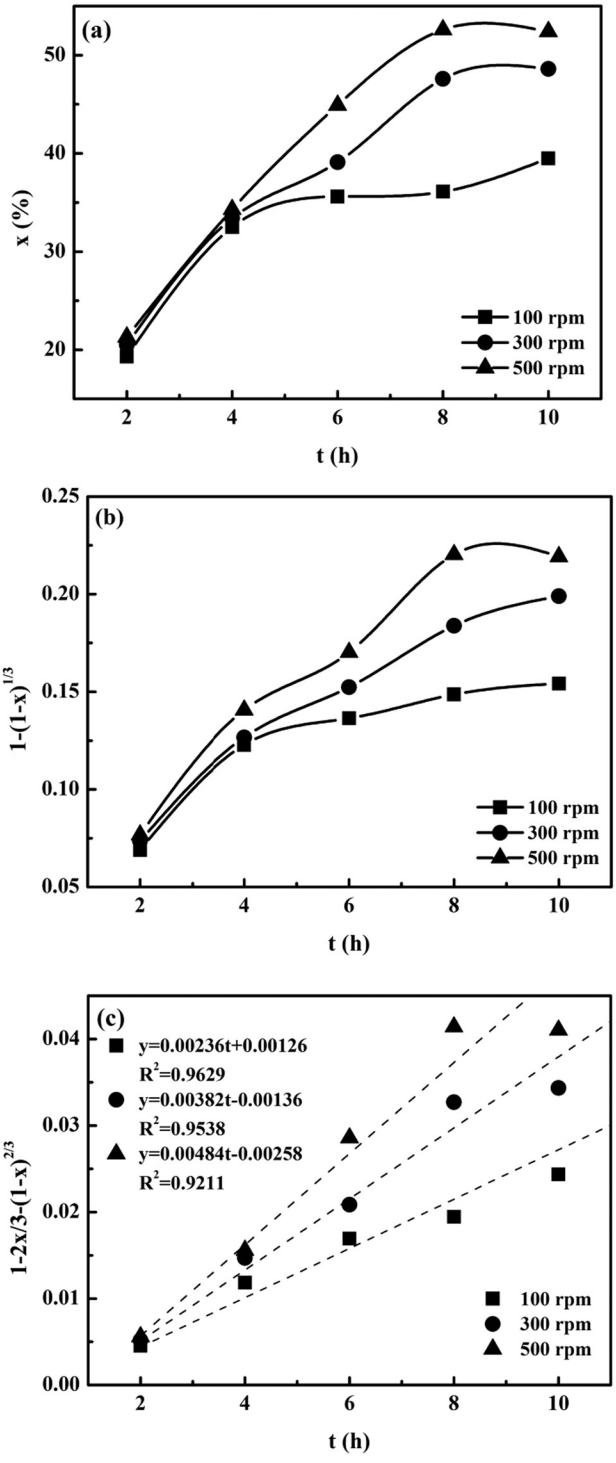

Figure 4: The relationship between (a) t and x, (b) t and $1-(1-x)^{1/3}$ (c) t and $1-\frac{2}{3}x-(1-x)^{2/3}$ without ultrasonic-assisted leaching (acid leaching conditions – $H_2C_2O_4$ concentration: 10 g/L, HCl concentration: 5%, L/S ratio: 5 and temperature: 60°C).

removal rate increases with increasing stirring speed. Assuming the chemical reaction as the rate-determining step, the relationship between the iron removal rate x and reaction time t can be given as equation (5). According to Figure 4(b), there is no linear relationship between $1-(1-x)^{1/3}$ and t. Hence, it can be judged that chemical reaction is not the rate-determining step. Similarly, assuming internal diffusion as the rate-determining step, the relationship between x and t can be given as equation (6), and there is a linear relationship between $1-\frac{2}{3}x-(1-x)^{2/3}$ and t, as shown in Figure 4(c). The curves were fitted by software Origin 8.0 and R^2 is greater than 0.92. This means that internal diffusion is the rate-determining step.

Figure 5 shows the results of ultrasonic-assisted acid leaching. The curve characteristics are similar to those of conventional acid leaching. Ultrasound agitation intensity increases with increasing ultrasonic input power, which is conducive to improve the mass transfer diffusion process [27].

Similarly, the iron removal rate x is substituted into Equations (5) and (6), respectively. The variations in $1-(1-x)^{1/3}$ and $1-\frac{2}{3}x-(1-x)^{2/3}$ with t are illustrated in Figure 5(b) and (c). As can be seen, each curve in Figure 5(c) shows a good linear relationship between $1-\frac{2}{3}x-(1-x)^{2/3}$ and t, and R^2 is greater than 0.90. Obviously, the rate-determining step of the ultrasound-assisted leaching process is still the internal diffusion. The experimental data are basically in line with the shrinking core model.

3.3 Calculation of apparent activation energy and derivation of mathematical model

The relationship between the chemical reaction rate constant k_d and temperature T can be explained by Arrhenius equation [28]:

$$k_d = A\exp\left(-\frac{E_a}{RT}\right) \tag{7}$$

where A is the pre-exponential factor, E_a is the apparent activation energy, R is the molar gas constant 8.314 J/(mol K) and T is the thermodynamic temperature.

The logarithm form of Equation (7) is given as

$$\ln k_d = \ln A - \frac{E_a}{R}\times\frac{1}{T} \tag{8}$$

A clear linear relationship can be observed between $\ln k_d$ and $\frac{1}{T}$. The slope of the line is recorded as k', and then the E_a is given as

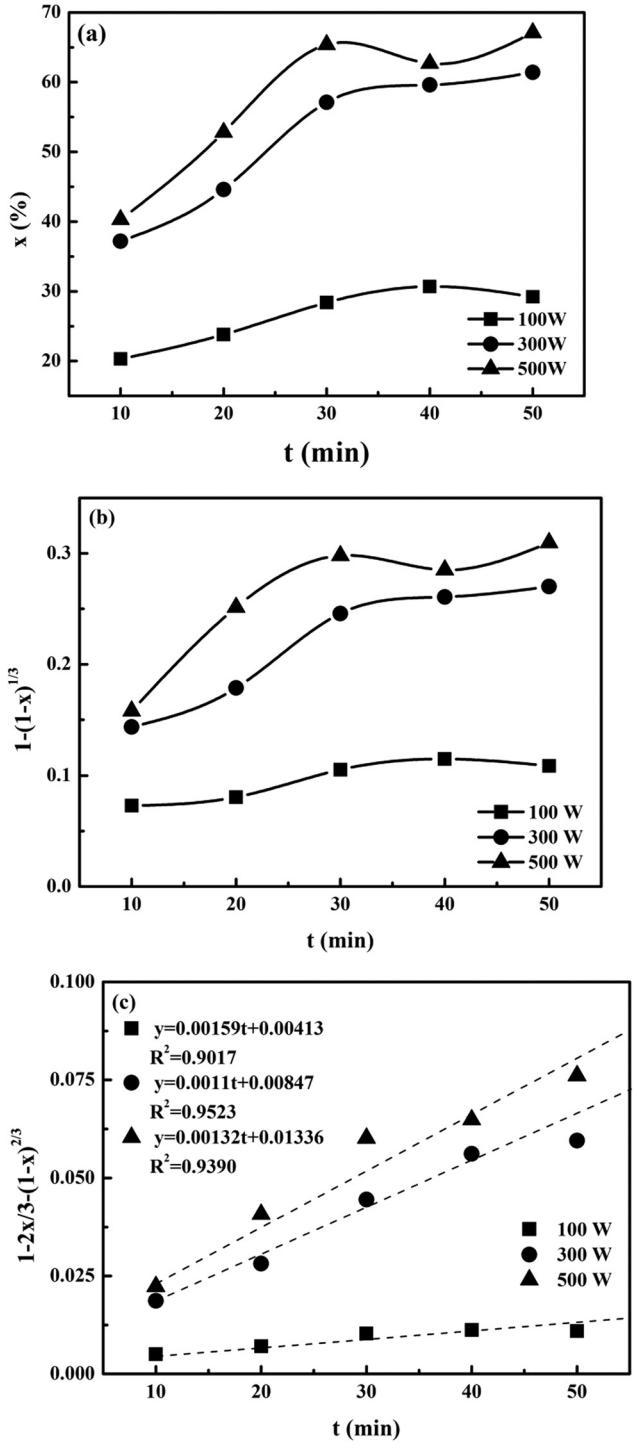

Figure 5: The relationship between (a) t and x, (b) t and $1-(1-x)^{1/3}$ (c) t and $1-\frac{2}{3}x-(1-x)^{2/3}$ with ultrasonic-assisted leaching (acid leaching conditions – $H_2C_2O_4$ concentration: 10 g/L, HCl concentration: 5%, L/S ratio: 5 and temperature: 60°C).

$$E_a = Rk' \tag{9}$$

Figure 6(a) shows the effects of reaction temperature on the iron removal rate under the condition without ultrasound. It can be seen that the temperature rise can facilitate the leaching efficiency.

The calculated results according to equation (5) are presented in Figure 6(b), and the Arrhenius plot is given in Figure 6(c). According to equation (9),

$$E_a = 2458.72 \times 8.314 = 20441.78 \text{ J/mol}, \quad \text{i.e.}$$
$$E_a = 20.44 \text{ kJ/mol}.$$

Thus, the kinetic equation for explaining the effects of reaction temperature on iron removal can be derived as:

$$\ln k_d = 1.586 - 2458.72 \times \frac{1}{T} \tag{10}$$

or

$$k_d = \exp\left(1.586 - 2458.72 \times \frac{1}{T}\right) \tag{11}$$

According to equations (6) and (11), a mathematical model for iron removal can be obtained:

$$1 - \frac{2}{3}x - (1-x)^{2/3} = \exp\left(1.586 - 2458.72 \times \frac{1}{T}\right) \times t \tag{12}$$

Similarly, the effects of reaction temperature on the iron removal rate the under ultrasonic-assisted leaching were studied, and the results are shown in Figure 7(a). As can be seen, ultrasonic-assisted leaching induces a remarkable acceleration of the iron removal rate, which can be up to 74% in only 40 min. By contrast, the conventional stirring method takes more than 8 h to reach the maximum.

The relationships between $1 - \frac{2}{3}x - (1-x)^{2/3}$ and t and between $\ln k_d$ and $\frac{1}{T}$ are plotted in the same procedure as described above, and the results are shown in Figure 7(b) and (c), respectively. According to equation (9),

$$E_a = 3333.56 \times 8.314 = 27715.22 \text{ J/mol}, \quad \text{i.e.}$$
$$E_a = 27.72 \text{ kJ/mol}.$$

It is well-known that the apparent activation energy of chemical reaction is usually in the range of 40–400 kJ/mol. In this study, the calculated activation energies under the conditions of regular leaching and ultrasonic-assisted leaching are both less than the lower limiting value. This further proves that the rate-determining step of the process is internal diffusion.

The kinetic equation for explaining the effects of reaction temperature on iron removal under the ultrasound-assisted leaching can be derived as:

$$\ln k_d = 3.647 - 3333.56 \times \frac{1}{T} \tag{13}$$

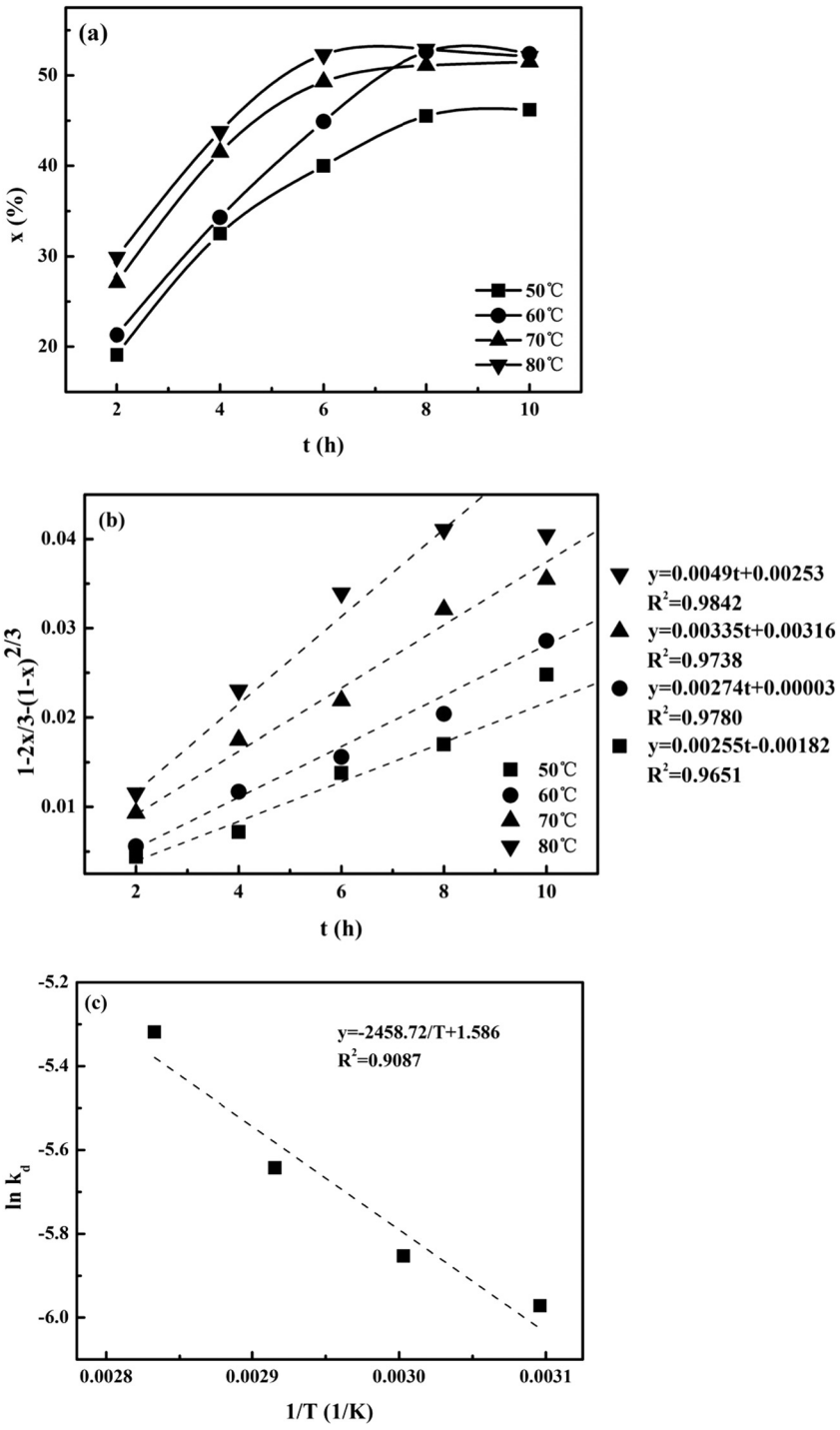

Figure 6: The relationship between (a) t and x, (b) t and $1 - \frac{2}{3}x - (1 - x)^{2/3}$ and (c) $\frac{1}{T}$ and $\ln k_d$ (acid leaching conditions – $H_2C_2O_4$ concentration: 10 g/L, HCl concentration: 5%, L/S ratio: 5 and stirring speed: 500 rpm).

Thus, a mathematical model for iron removal under the ultrasound-assisted leaching can be derived as:

$$1-\frac{2}{3}x-(1-x)^{2/3}=\exp\left(3.647-3333.56\times\frac{1}{T}\right)\times t \quad (14)$$

3.4 Calculation of apparent activation energy

High-purity quartz product was obtained under the optimal parameters, i.e., an oxalic acid concentration

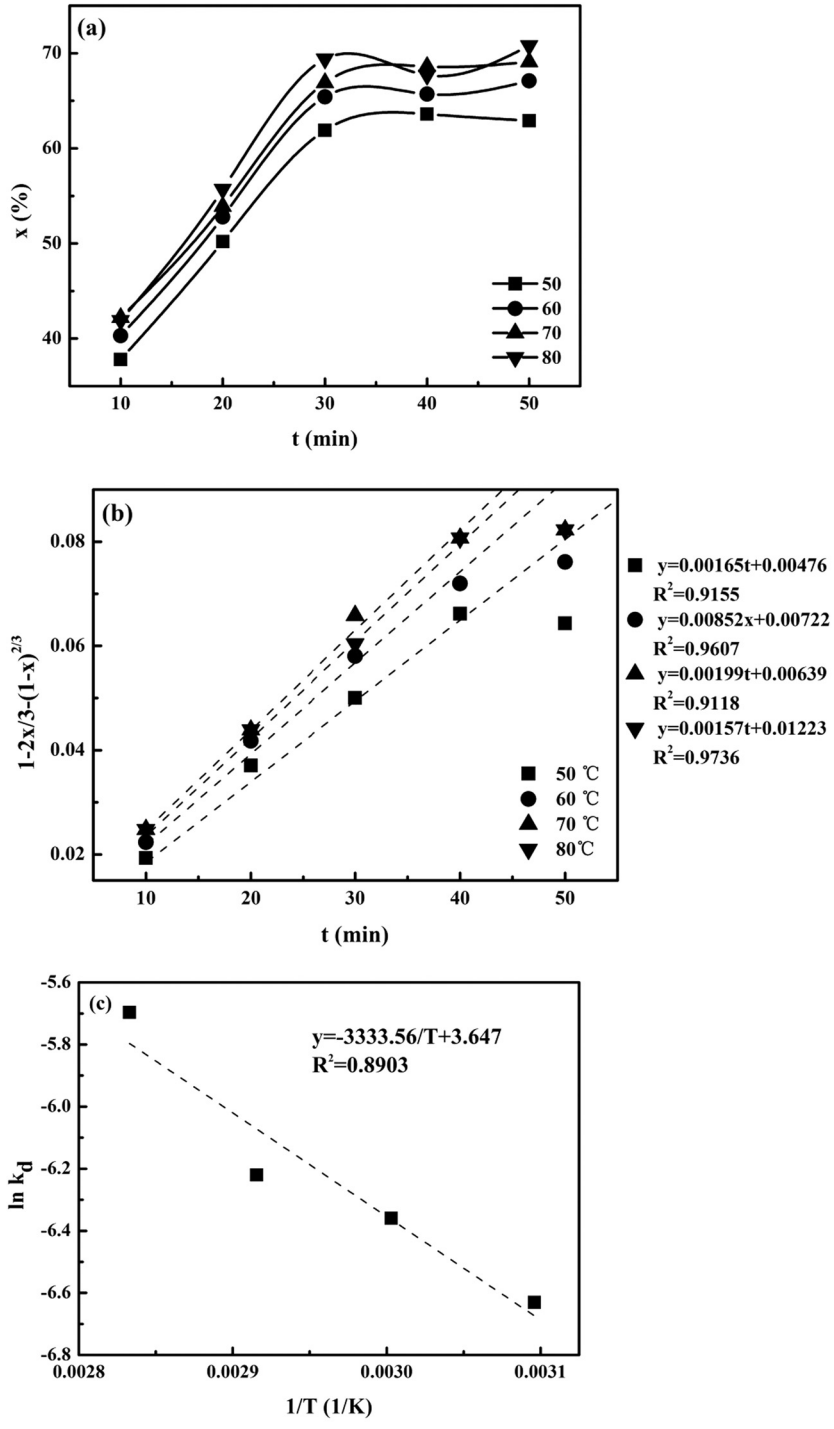

Figure 7: The relationship between (a) t and x, (b) t and $1 - \frac{2}{3}x - (1 - x)^{2/3}$ and (c) $\frac{1}{T}$ and $\ln k_d$ (acid leaching conditions – $H_2C_2O_4$ concentration: 10 g/L, HCl concentration: 5%, L/S ratio: 5 and ultrasonic input power: 500 W).

Table 2: The chemical composition of concentrate samples by XRF (%)

Components	SiO_2	Al_2O_3	Fe_2O_3	CaO	Na_2O	K_2O	MgO
Amount	99.9047	0.0810	0.0223	0.0106	0.0194	0.0189	0.0213

of 10 g/L, a hydrochloric acid concentration of 5%, an extraction temperature of 60°C, a liquid–solid ratio of 5, an ultrasound power of 400 W and an ultrasound treatment time of 30 min. The SiO_2 content was increased from 99.5828% to 99.9047%, Fe_2O_3 content was reduced from 0.0857% to 0.0223% and a maximal iron removal rate of up to 74%. The chemical composition of the concentrates is shown in Table 2.

4 Conclusions

The kinetics of iron removal from quartz under the ultrasound-assisted leaching had been investigated. The results showed that the iron removal efficiency increased with increasing temperature, stirring speed or ultrasonic input power. The leaching time could be greatly shortened under ultrasonic-assisted leaching compared with the regular stirring method, and the maximum iron removal rate of 74% was achieved in only 40 min. Under the optimal parameters, the SiO_2 content of the concentrates increased from 99.5828% to 99.9047% and the Fe_2O_3 content reduced from 0.0857% to 0.0223%. The experimental data fitted well with the shrinking core model for the internal diffusion-controlled leaching process. The apparent activation energy of the reaction under the ultrasound-assisted leaching was $E_a = 27.72$ kJ/mol, and the mathematical model for iron removal can be derived as:

$$1 - \frac{2}{3}x - (1 - x)^{2/3} = \exp\left(3.647 - 3333.56 \times \frac{1}{T}\right) \times t$$

References

[1] Zou, X. L., L. Ji, J. B. Ge, D. R. Sadoway, E. T. Yu, and A. J. Bard. Electrodeposition of crystalline silicon films from silicon dioxide for low-cost photovoltaic applications. *Nature Communications*, Vol. 10, 2019, pp. 1–7.

[2] Rao, C. N. R., H. S. S. Ramakrishna Matte, K. S. Subrahmanyam, and U. Maitra. Unusual magnetic properties of graphene and related materials. *Chemical Science*, Vol. 3, 2012, pp. 45–52.

[3] Larsen, E., and R. A. Kleiv. Flotation of quartz from quartz-feldspar mixtures by the HF method. *Minerals Engineering*, Vol. 98, 2016, pp. 49–51.

[4] Zhang, Z. Z., J. S. Li, X. X. Li, H. Q. Huang, L. F. Zhou, and T. T. Xiong. High efficiency iron removal from quartz sand using phosphoric acid. *International Journal of Mineral Processing,* Vol. 114–117, 2012, pp. 30–34.

[5] Vatalis, K. I., G. Charalambides, and N. P. Benetis. Market of high purity quartz innovative applications. *Procedia Economics and Finance*, Vol. 24, 2015, pp. 734–742.

[6] Kefaifi, A., T. Sahraoui, A. Kheloufi, and E. Bobocioiu. Optimization of quartz sand leaching process using design experiments method (DOE). *Silico*, Vol. 11, 2019, pp. 1481–1488.

[7] Tuncuk, A., and A. Akcil. Iron removal in production of purified quartz by hydrometallurgical process. *International Journal of Mineral Processing*, Vol. 153, 2016, pp. 44–50.

[8] Santos, M. F. M., E. Fujiwara, E. A. Schenkel, J. Enzweiler, and C. K. Suzuki. Processing of quartz lumps rejected by silicon industry to obtain a raw material for silica glass. *International Journal of Mineral Processing*, Vol. 135, 2015, pp. 65–70.

[9] Tuncuk, A., and A. Akcil. Removal of iron from quartz ore using different acids: a laboratory-scale reactor study. *Mineral Processing and Extractive Metallurgy Review*, Vol. 35, 2014, pp. 217–228.

[10] Du, F. H., J. S. Li, X. X. Li, and Z. Z. Zhang. Improvement of iron removal from silica sand using ultrasound-assisted oxalic acid. *Ultrasonics Sonochemistry*, Vol. 18, 2011, pp. 389–393.

[11] Farmer, A. D., A. F. Collings, and G. J. Jameson. Effect of ultrasound on surface cleaning of silica particles. *International Journal of Mineral Processing*, Vol. 60, 2000, pp. 101–113.

[12] Zhou, H. M., P. Lv, H. Qi, J. Q. Ma, J. J. Wang. Removal of residual functionalized ionic liquids from water by ultrasound-assisted zero-valent iron/activated carbon. *Environmental Technology*, Vol. 40, 2019, pp. 2504–2512.

[13] Li, X., P. F. Xing, X. H. Du, S. B. Gao, and C. Chen. Influencing factors and kinetics analysis on the leaching of iron from boron carbide waste-scrap with ultrasound-assisted method. *Ultrasonics Sonochemistry*, Vol. 38, 2017, pp. 84–91.

[14] Cornell, R. M., and P. W. Schindler. Photochemical dissolution of goethite in acid/oxalate solution. *Clays and Clay Minerals*, Vol. 35, 1987, pp. 347–352.

[15] Liu, K., Q. Y. Chen, Z. L. Yin, H. P. Hu, and Z. Y. Ding. Kinetics of leaching of a Chinese laterite containing maghemite and magnetite in sulfuric acid solutions. *Hydrometallurgy,* Vol. 125–126, 2012, pp. 125–136.

[16] Taxiarchou, M., D. Panias, I. Douni, I. Paspaliaris, and A. Kontopoulos. Dissolution of hematite in acidic oxalate solutions. *Hydrometallurgy*, Vol. 44, 1997, pp. 287–299.

[17] Lee, S. O., T. Tran, Y. Y. Park, S. J. Kim, and M. J. Kim. Study on the kinetics of iron oxide leaching by oxalic acid. *International Journal of Mineral Processing*, Vol. 80, 2006, pp. 144–152.

[18] Lee, S. O., T. Tran, B. H. Jung, S. J. Kim, and M. J. Kim. Dissolution of iron oxide using oxalic acid. *Hydrometallurgy*, Vol. 87, 2007, pp. 91–99.

[19] Olvera-Venegas, P. N., L. E. Hernández-Cruz, and G. T. Lapidus. Leaching of iron oxides from kaolin: Synergistic effect of citrate-thiosulfate and kinetic analysis. *Hydrometallurgy*, Vol. 171, 2017, pp. 16–26.

[20] Salmimies, R., P. Vehmaanperä, and A. Häkkinen. Acidic dissolution of magnetite in mixtures of oxalic and sulfuric acid. *Hydrometallurgy*, Vol. 163, 2016, pp. 91–98.

[21] Panias, D., M. Taxiarchou, I. Paspaliaris, and A. Kontopoulos. Mechanisms of dissolution of iron oxides in aqueous oxalic acid solutions. *Hydrometallurgy*, Vol. 42, 1996, pp. 257–265.

[22] Ahn, H., and S. Choi. A comparison of the shrinking core model and the grain model for the iron ore pellet indurator simulation. *Computers & Chemical Engineering*, Vol. 97, 2017, pp. 13–26.
[23] Astuti, W., T. Hirajima, K. Sasaki, and N. Okibe. Kinetics of nickel extraction from Indonesian saprolitic ore by citric acid leaching under atmospheric pressure. *Minerals & Metallurgical Processing*, Vol. 32, 2015, pp. 176–185.
[24] Zhukov, V. V., A. Laari, M. Lampinen, and T. Koiranen. A mechanistic kinetic model for direct pressure leaching of iron containing sphalerite concentrate. *Chemical Engineering Research and Design*, Vol. 118, 2017, pp. 131–141.
[25] Huang, Y. K., Z. H. Dou, T. A. Zhang, and J. Liu. Leaching kinetics of rare earth elements and fluoride from mixed rare earth concentrate after roasting with calcium hydroxide and sodium hydroxide. *Hydrometallurgy*, Vol. 173, 2017, pp. 15–21.
[26] Zhang, B., M. Li, X. W. Zhang, and J. Huang. Kinetics of uranium extraction from uranium tailings by oxidative leaching. *Journal of Operations Management*, Vol. 68, 2016, pp. 1990–2001.
[27] Chung, K. W., C. J. Kim, and H. S. Yoon. Enhanced ionic exchange of uranium by indirect ultrasonic application with a submerged ultrasound probe. *Minerals & Metallurgical Processing*, Vol. 32, 2015, pp. 230–234.
[28] Naveršnik, K., and R. Jurečič. Humidity-corrected Arrhenius equation: The reference condition approach. *The International Journal of Pharmaceutics*, Vol. 500, 2016, pp. 360–365.